Layered polymorph of titanium triiodide

Danrui Ni,[1] Ranuri S. Dissanayaka Mudiyanselage [•],[2] Xianghan Xu [•],[1] Junsik Mun,[4]
Yimei Zhu,[4] Weiwei Xie,[3] and R. J. Cava[1]

[1]*Department of Chemistry, Princeton University, Princeton, New Jersey 08544, USA*
[2]*Department of Chemistry and Chemical Biology, Rutgers University, Piscataway, New Jersey 08854, USA*
[3]*Department of Chemistry, Michigan State University, 578 South Shaw Lane, East Lansing, Michigan 48824, USA*
[4]*Condensed Matter Physics and Materials Science Department, Brookhaven National Laboratory, Upton, New York 11973, USA*

A previously unreported layered triangular lattice polymorph of TiI_3 is described, synthesized under 6 GPa of applied pressure at $900\,°C$, but stable at atmospheric pressure. This air-sensitive material has a CdI_2-type layered structure [$P-3m1$ (no. 164), $a = 4.012$ Å and $c = 6.641$ Å at 120 K, $Z = 1$ of $Ti_{0.667}I_2$] with an in-plane triangular lattice, related to that of TiI_4 ($Ti_{0.5}I_2$). Although the TiI_3 formula is consistent with expectations for a layered honeycomb lattice of spin 1/2 Ti(III), there is disorder in the crystal structure, and the complex magnetic behavior observed is inconsistent with a simple local moment picture of spin 1/2 per Ti(III). Magnetic susceptibility and heat capacity measurements suggest that the material undergoes several low-temperature phase transitions.

I. INTRODUCTION

Metal halides, especially transition-metal halides, have attracted much research interest in recent years. Many members in this large family including three-dimensional (3D) perovskites [1], 2D layers (triangular [2,3], kagomé [4], or honeycomb [5–7]), and 1D chains [8,9], have been reported. Polymorphic behavior is also known [10–12]. The materials can display unexpected physical and/or photochemical properties, and thus promising performance in photovoltaic, electric, and quantum material applications [13–16]. It is therefore of great interest to characterize new phases of transition-metal halides and study their physical and chemical properties. Here we describe the disordered layered triangular lattice material TiI_3, which, in a localized electron model, would have one unpaired electron, spin 1/2, synthesized at 6 GPa. Its crystal structure is very different from that of the ambient pressure synthesized phase, which is made from titanium iodide chains.

Among the reported transition-metal trihalides, $TiCl_3$, with Ti^{3+} in a d^1 configuration, was found to have both layered and chain-structure polymorphs as early as 1961 [10]. The triiodide variant, TiI_3, however, has only been reported to display a 1D chain structure. Iodides can display properties that are much different from their chloride cousins and are therefore worth finding [17], and a potential two-dimensional phase consisting of spin 1/2 metals in a layered lattice with iodine atoms is theoretically expected to display interesting electronic and magnetic properties [18]. The layered polymorph of spin 1/2 TiI_3 has not been reported experimentally until now. We report it here but find it to display a disordered Ti sublattice when synthesized under our conditions, which may be due to either stacking faults or in-plane Ti-vacancy disorder, the latter being the most likely.

As a starting point for understanding the synthesis of the current material, we note that pressure-induced polymorphism has been reported in the well-studied ruthenium trihalides. While $RuCl_3$ undergoes a phase transition from its chain-structure β-phase to a honeycomb-layered α-phase with increasing temperature, for its sister compounds $RuBr_3$ and RuI_3 only chain structures have been reported at ambient pressure; with the help of applied pressure, however, the honeycomb layer polymorphs of $RuBr_3$ and RuI_3 have been experimentally synthesized [17,19,20]. In that vein, here we employ modest temperatures and pressures to synthesize a layered polymorph of TiI_3 which in a localized electron model would have spin 1/2 Ti (III). Layered TiI_3 is air-sensitive (as is the ambient pressure polymorph) and is refined to have a P-$3m1$ CdI_2-type structure with Ti(III) on average partially occupying 2/3 of the Cd-type sites. This material is structurally related to the $d°$ compound TiI_4 ($Ti_{0.5}I_2$) whose structure consists of zigzag chains of edge-shared TiI_6 octahedra within a layered iodine array. Possible explanations for the partial occupancy of titanium in the triangular layered lattice are discussed, and magnetic susceptibility and heat capacity measurements are carried out, suggesting the presence of phase transitions in TiI_3 in the lower temperature range.

II. EXPERIMENT

The ambient-pressure phase of TiI_3, used as a starting material, was synthesized using elemental titanium powder (Alfa Aesar, 99.9%) and iodine (Sigma Aldrich, 99.99%). It was annealed in vacuum in sealed quartz tubes for three days, with multiple annealing temperatures between 300 and $700\,°C$ tested to increase the yield. Some impurities were produced during the annealing, including TiI_4, and TiI_2. A

low-temperature vapor transport method was used for purification before the high-pressure synthesis. With the hot zone kept at 350 °C, impurities such as TiI_4 are transferred to the cold end, leaving pure TiI_3 in the region with higher temperature. The resulting black-colored, 1D-chain structure TiI_3 material was used as a starting material for the high-pressure synthesis. TiI_4 was also employed for high-pressure synthesis experiments, as described below.

The ground powder of the starting material was loaded into a boron nitride crucible and then inserted into a pyrophyllite cube assembly. The samples were pressed to 6 GPa using a cubic multi-anvil system (Rockland Research Corp.) and annealed at different temperatures (700–1000 °C), with the temperature measured by an internal thermocouple. The samples were then quench-cooled to ambient temperature before decompression. Annealing at 900 °C for 1 h gave the best results. The products obtained displayed a black color. Small single crystals were picked up in the postreaction samples and were used for single-crystal x-ray diffraction (SCXRD) characterization of the crystal structure. All the titanium iodide compounds prepared require handling in an air-free atmosphere. Thus, the PXRD patterns used for characterization were collected using a Rigaku Miniflex II diffractometer located inside a nitrogen-filled glove box. Cu $K\alpha$ radiation ($\lambda = 1.5406$ Å) was employed, and Le Bail fitting of the acquired patterns, when performed, was conducted via the TOPAS software.

SCXRD data of TiI_3 crystals were collected at 120 K on a Bruker D8 Quest Eco using graphite-monochromated Mo $K\alpha$ radiation ($\lambda = 0.71073$ Å). A liquid-nitrogen stream was used to prevent samples from decomposing. The frames were integrated using the SAINT program within the APEX III 2017.3-0 operating system. The structure was determined using direct methods and difference Fourier synthesis (SHELXTL version 6.14) [21]. The P-3m1 (no. 164) space group was suggested by XPREP. Other potential space groups (P-31c, $P63mc$, $P63/mmc$, and $P6/mmm$) were also tested, but structures in those space groups did not lead to satisfactory or better refinements, with either higher $R/wR2$ or higher R_{int} values. The electron microscopy measurements were conducted on ground powder of TiI_3, but the beam-sensitivity of the sample significantly limited its characterization by this method.

The extreme air sensitivity of the high-pressure-synthesized compound makes getting quantitative magnetic susceptibility and heat capacity data difficult, but magnetization and heat capacity measurements were conducted in any case, with an effort made to minimize contact of the material with air. The experiments were carried out using a Quantum Design PPMS (Dynacool), equipped with a vibrating sample magnetometer (VSM) option. For these and all other cases, transfers were performed very rapidly to prevent sample decomposition. Magnetic susceptibility was defined as M/H, and the temperature-dependent magnetization (M) was measured in an applied magnetic field (H) of 1000 Oe.

III. RESULTS AND DISCUSSION

1D chain TiI_3 ($Pmnm$ [22]) and cubic TiI_4 (Pa-3 [23]) were synthesized and purified at ambient pressure, and they were used as starting materials for the high-pressure

TABLE I. Single-crystal structure refinement for HP-TiI_3. (Standard deviation is indicated by the values in parentheses.)

Empirical formula	$Ti_{0.67}I_2$
Temperature (K)	120(2)
Crystal system	Trigonal
Space group	P-3m1 (no. 164)
Z	1
F.W. (g/mol)	285.89
a(Å)	4.0118(6)
c(Å)	6.6409(13)
V(Å^3)	92.56(3)
F(000)	121
θ range (deg)	3.067–26.367
Number of reflections	416 ($R_{int} = 0.0161$)
Independent reflections	95
Number of parameters	6
Goodness-of-fit on F^2	1.368
Final R indices [$I > \sigma$(I)]	$R1 = 0.0316$, $wR2 = 0.0773$
R indices (all data)	$R1 = 0.0318$, $wR2 = 0.0774$
Largest diff. peak and hole (e^-/Å^3)	2.911; –1.420

synthesis (Figs. S1 and S2 of the Supplemental Material [35] show their ambient temperature PXRD patterns). Optimized synthesis conditions for the high pressure TiI_3 phase were found to be 900 °C and 6 GPa for 1 h. The high-pressure TiI_3 phase (HP-TiI_3) obtained crystallizes in a layered structure in the P-3m1 space group (no. 164) with $a = 4.012$ Å and $c = 6.641$ Å at 120 K (Fig. 1). The crystallographic information is presented in Tables I–III and Table S1 in the Supplemental Material [35]. During the refinement, pseudosymmetry elements (i.e., a 6_3 screw and a c glide) were suggested by Checkcif, but they were found not to be present. The P-3m1 structure yields the best refinement. The hk0, hk1, and $0kl$ reciprocal planes of HP-TiI_3 are shown in Fig. 2(a).

HP-TiI_3 crystallizes in a CdI_2-type layered structure with a triangular lattice, where the Ti on average randomly occupies the Cd site, leading to an occupancy ratio of 0.667Ti:2I when considered on an MX_2 structural basis. Compared to the low-temperature structure of ambient pressure chained TiI_3, which was reported at approximately the same temperature [22], the TiI_6 octahedra in the HP material are less distorted. The Ti-I bond length is about 2.82 Å, and the TiI_6 polyhedron is closer to that of a regular octahedron. When compared to high-temperature chain-structure AP-TiI_3 ($P63/mcm$ space group with more symmetric Ti-coordination), the bonding distance is slightly longer in HP-TiI_3 (Table III). The 300 K PXRD pattern of HP-TiI_3 is consistent with the SCXRD results (confirmed by Le Bail fitting in Fig. S3 [35]), yielding an a of 4.0277(2) Å and a c of 6.6828(2) Å at 300 K for the P-3m1 unit cell. A small amount of ambient pressure TiI_3 is found in the HP-TiI_3 PXRD pattern—less than 9% based on a rough Rietveld refinement.

After an analogous high-pressure high-temperature treatment, TiI_4 shows a PXRD pattern that indicates that it also has a trigonal crystal structure. Some impurities remain present, including monoclinic TiI_4, whose crystal structure [24] is closely related to that of trigonal HP-TiI_3. 1D chain TiI_3 and
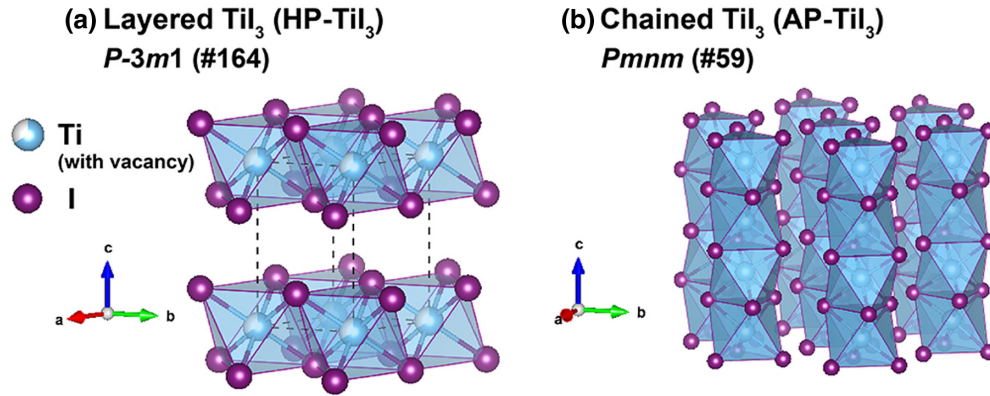
FIG. 1. The crystal structures of TiI_3. (a) The average P-$3m1$ unit cell of HP-TiI_3, refined from SCXRD measurements; (b) the $Pmnm$ unit cell of the 1D-chain structure of AP-TiI_3 [22]. Titanium is represented by the light blue spheres and iodine by the purple spheres, while vacancies are shown by white.

titanium metal are also present (Fig. S4 [35]). The cubic TiI_4 polymorph, which was the starting material for the HP synthesis, is reported to be metastable at 300 K, slowly transforming to monoclinic TiI_4 at ambient pressure [23], so it is not surprising that this phase was not observed in the postreaction PXRD pattern. By viewing the PXRD patterns of the high-pressure synthesized TiI_3 and TiI_4 together [Fig. 2(b)], small shifts of the peaks are revealed. The similar diffraction patterns suggest that HP-TiI_4 and HP-TiI_3 are essentially isostructural, but that due to the different Ti:I ratios in the starting materials, HP-TiI_4 has a different occupancy of Ti on the $1a$ Wyckoff site in the crystal structure. The Le Bail fitting of the 300 K PXRD pattern for HP-TiI_4 yields $a = 4.0178(2)$ Å and $c = 6.6299(3)$ Å, with these smaller values being consistent with the expected lower radius of d^0 Ti^{4+} compared to that of d^1 Ti^{3+}. This structure type has also been observed for TeI_4 [25], as one of its polymorphs was found to adopt a CdI_2-type structure ($Te_{0.5}I_2$) with a random distribution of Te and vacancies over the potential metal positions in the layered triangular lattice. Another comparable example is Os_xCl_3 [26,27], which will be discussed in a later section. Based on the similarity of the two PXRD patterns, the HP titanium iodide series in the composition range studied may be a solid solution with the same P-$3m1$ layered structure but with different Ti content on the $1a$ site, i.e., resulting in an average formula of Ti_xI_2, with x varying at least between 0.5 and 0.667. As some reports suggest that TiI_2 also crystallizes in a CdI_2-type structure [28], the range of possible x values may be even larger, 0.5–1.

Thus, TiI_3 undergoes a phase transition from a 1D chain structure [Fig. 1(b)] to a layered one at high pressures and temperatures. Similar polymorphism has been reported for $RuBr_3$ and RuI_3 [17,19,20]. The layered polymorphs of these compounds usually adopt a honeycomb Ru sublattice,

however. As shown in Figs. 3(a) and 3(b), while a fully occupied triangular lattice leads to a 1:2 cation-to-anion ratio (i.e., a CdI_2 type structure), a honeycomb arrangement is an ordered 2/3 filled triangular lattice, resulting in a 0.667:2 = 1:3 formula (BiI_3 type), and a crystallographic cell in the basal plane that is about $\sqrt{3}$ larger than that observed here. We see no indication of this supercell in our diffraction patterns—in TiI_3 synthesized by our method, in contrast, it appears that the Ti atoms are on average randomly distributed on the metal ($1a$) sites of the triangular lattice. This may either be a truly random arrangement of Ti in the plane, or it may be that the local structure is still honeycomb-like in the plane with errors in the plane-stacking, making the average structure appear to be trigonal with a smaller in-plane cell. (SCXRD measurements are a positional average over the whole crystal, and thus a random layer stacking can give rise to a triangular reciprocal lattice in plane, with an equal occupancy fraction on each site of $Ti_{0.667}$.) This explanation can also work for the HP-TiI_4 case. The thermodynamically stable phase of TiI_4 at ambient pressure has been refined to have $C2/c$ symmetry [24], and when ignoring the slight distortion of TiI_6 octahedra, this structure can be considered as stacked $Ti_{0.5}I_2$ planes, with zigzag chains of edge sharing TiI_6 octahedra in the basal-plane alternating with empty octahedra of similar geometry, as shown in Fig. 3(c). These intralayer zigzag chains can be regarded as a 1/2 filled triangular lattice, matching the 0.5:2 = 1:4 formula. After annealing at high temperature and high pressure, the structure of TiI_4 appears to be less distorted, with more stochastic stacking of the planes, which are now more regularly stacked. Thus, the PXRD pattern of HP-TiI_4 reflects an average structure close to that of HP-TiI_3, but with different Ti fraction and different lattice parameters. Based on the SCXRD characterization of HP-TiI_3, however, evidence

TABLE II. Atomic coordinates and equivalent isotropic displacement parameters of HP-TiI_3 at 120(2) K. [U_{eq} is defined as one-third of the trace of the orthogonalized U_{ij} tensor (Å^2).]

Atom	Wyckoff	Occ.	x	y	z	U_{eq}
Ti1	$1a$	0.6667	0	0	0	0.0166(19)
I1	$2d$	1	0.666 667	0.333 333	0.757 15(19)	0.0125(5)

TABLE III. Selected bond lengths and bond angles for HP-TiI$_3$ [this work, refined at 120(2) K] and 1D-chain structure AP-TiI$_3$; low-temperature phase (LT) reported at 100 K and high-temperature phase (HT) reported at 326 K [22]. (Standard deviation is indicated by the values in parentheses.)

	HP-TiI$_3$		AP-TiI$_3$ (LT) [22]		AP-TiI$_3$ (HT) [22]	
Space group	*P*-3*m*1 (no. 164)		*Pmnm* (no. 59)		*P*6$_3$/*mcm* (no. 193)	
Temp (K)	120(2)		100		326	
Bond length (Å)	Ti1-I1 (×6)	2.8224(8)	Ti1-I1 (×2)	2.7433(6)	Ti1-I1 (×6)	2.7885(3)
			Ti1-I2 (×2)	2.8318(6)		
			Ti1-I3 (×1)	2.7420(8)		
			Ti1-I4 (×1)	2.8346(8)		
Bond angle (deg)	I1-Ti1-I1 (×6)	90.58(3)	I1-Ti1-I1 (×1)	93.83(3)	I1-Ti1-I1 (×6)	90.630(7)
	I1-Ti1-I1 (×6)	89.42(3)	I1-Ti1-I2 (×2)	90.025(11)	I1-Ti1-I1 (×6)	89.370(7)
	I1-Ti1-I1 (×3)	180.0	I1-Ti1-I3 (×2)	93.48(2)	I1-Ti1-I1 (×3)	180.0
			I1-Ti1-I4 (×2)	90.405(19)		
			I2-Ti1-I2 (×1)	85.82(3)		
			I2-Ti1-I3 (×2)	90.545(18)		
			I2-Ti1-I4 (×2)	85.291(17)		
			I1-Ti1-I2 (×2)	174.24(3)		
			I3-Ti1-I4 (×1)	174.31(3)		

for the presence of interlayer stacking faults [streaks can be observed in the 0*kl* reciprocal plane in Fig. 2(a), compared to the *hk*0 and *hk*1 planes] is relatively weak, and different from the expectation that there should be stronger streaking along *l* for interlayer stacking errors (also see the electron microscopy result shown in Fig. S5 [35]). This observation makes in-plane disorder more likely. Characterization of the potential stacking faults, short-range in-plane Ti-vacancy arrangements, and

the symmetry of smaller domains in both TiI$_3$ and TiI$_4$ may therefore be of future interest.

The resistance of dense polycrystalline pellets of HP-TiI$_3$ was too high to measure at room temperature, indicating that the material is either an insulator or a semiconductor. The magnetic behavior and thermal properties of layered HP-TiI$_3$ were also estimated. The magnetic susceptibility measured on a polycrystalline HP-TiI$_3$ powder sample from 1.8 to 300 K
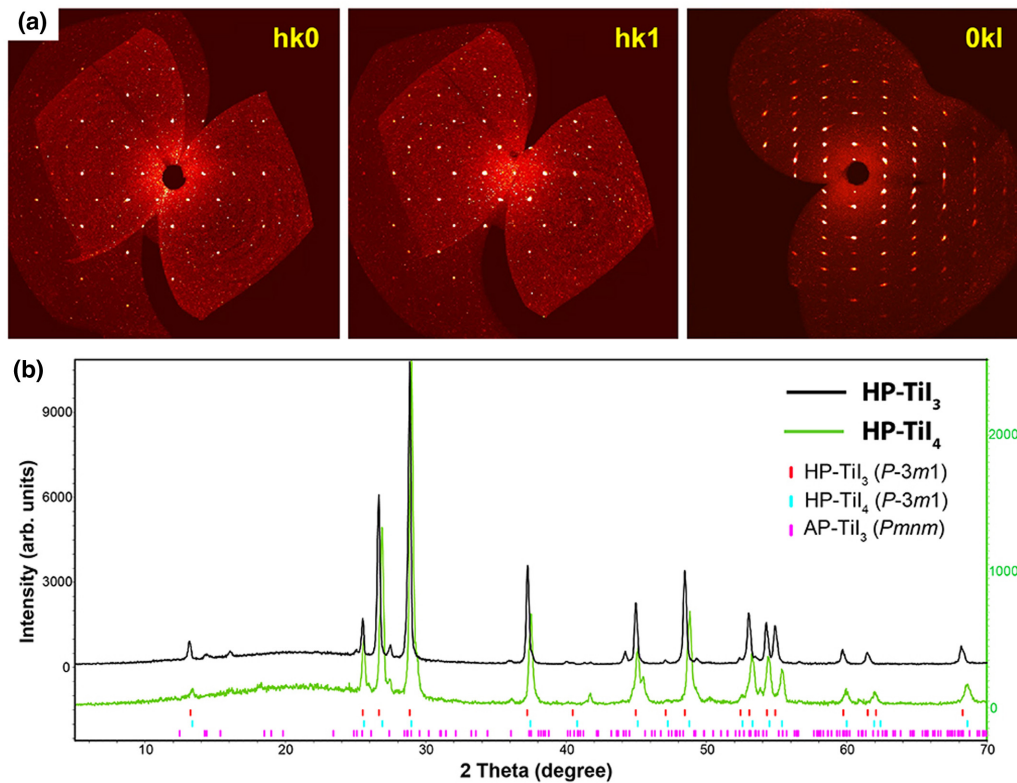

FIG. 2. The diffraction characterization of HP-TiI$_3$ and HP-TiI$_4$. (a) The *hk*0 (left), *hk*1 (middle), and 0*kl* reciprocal-lattice planes of single-crystal HP-TiI$_3$ at 120 K. (b) The laboratory PXRD patterns of HP-TiI$_3$ (black pattern with left *y*-axis) and HP-TiI$_4$ (green pattern with right *y*-axis), with the calculated Bragg reflection tics of HP-TiI$_3$, HP-TiI$_4$, and AP-TiI$_3$ as a small amount of impurity.

(a) Triangular Lattice (Fully occupied) **(b) Honeycomb Lattice (2/3 occupied)** **(c) In-plane Zigzag Chains (1/2 occupied)**
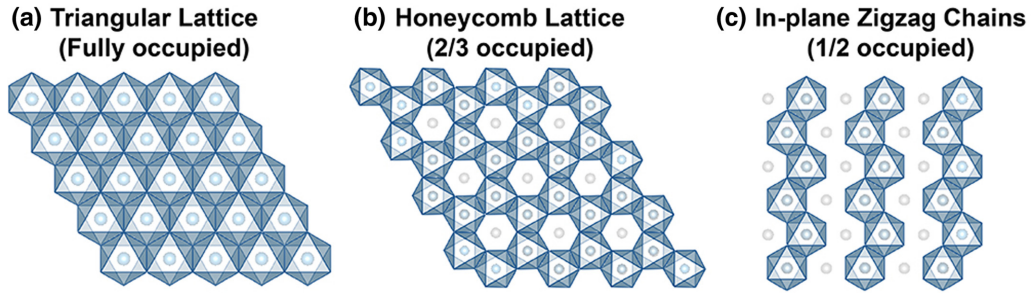
FIG. 3. Three different arrangements of the potential in-plane lattices. (a) A fully occupied triangular lattice (MX_2) of the CdI_2 type; (b) a 2/3 occupied honeycomb lattice (MX_3) as is observed for BiI_3, and (c) a 1/2 occupied in-plane zigzag chain lattice as is found for TiI_4 [3,14,24].

is shown in Fig. 4(a) (main panel), with data for 1D-chain structure ambient pressure AP-TiI$_3$ and HP-TiI$_4$ plotted in the same panel for comparison. In contrast to the other two materials, the behavior of HP-TiI$_3$ displays several features in the magnetic susceptibility below about 100 K, including a weak broad bump around 90 K, a feature around 45 K, and a transition at 22 K. These features are not observed in the χ versus T plots for either AP-TiI$_3$ or HP-TiI$_4$. This indicates that these magnetic properties of HP-TiI$_3$ may be correlated with its layered structure and the single unpaired electron of what is formally Ti(III). Structural disorder, hybridization between Ti and I, and a potential lattice distortion may introduce complexity in the magnetic behavior, however. Both zero-field-cooled (ZFC) and field-cooled (FC) data were collected on HP-TiI$_3$, and an obvious difference in the magnetic susceptibility measured in the ZFC and FC runs can be observed at temperatures below 20 K (Fig. S6 [35]).

Magnetization versus applied magnetic field data for HP-TiI$_3$ was collected at different temperatures; the curves at 2, 15, 22, 35, and 75 K are presented in Fig. 4(b). An S-shaped variation of M versus H, with hysteresis, can be clearly observed at 2 K, with a magnetization that saturates to values slightly above $0.1\mu_B$ per Ti (consistent with a canted-spin structure). The S-shape is also seen in the data taken at 15–35

K [Fig. 4(b), inset], shrinking with increasing temperature and becoming a straight line in the 75 K data. This suggests that there may be a ferromagnetic component or some spin-freezing or spin-glassiness component to the transition seen in the magnetic susceptibility. An x-ray diffraction study of a sample removed from the magnetometer under normal conditions showed the presence of some titanium (IV) iodide hydroxide hydrate [TiI(OH)$_3 \cdot x$H$_2$O] and iodine oxides in addition to the original HP-TiI$_3$ phase, as a result of the partial decomposition of the extremely air-sensitive material, and thus though the measured magnetic behavior can be considered as correct in general, we cannot guarantee that it is correct in detail.

We can speculate that the unusual magnetic behavior and the relatively low moment per mole of HP-TiI$_3$ [which in a localized picture would have spin 1/2 for each Ti(III)] may be due to multiple possible factors, including structural disorder of the metal cations and vacancies, Ti-I hybridization, and the in-plane lattice symmetry at low temperature (especially the potential for structural Ti dimerization), as symmetry breaking and dimerization of Ti(III) cations has been observed and reported for chain structured AP-TiI$_3$. It has been suggested that the distortion and breaking of intralayer trigonal symmetry can lead to significant effects on the electric and magnetic
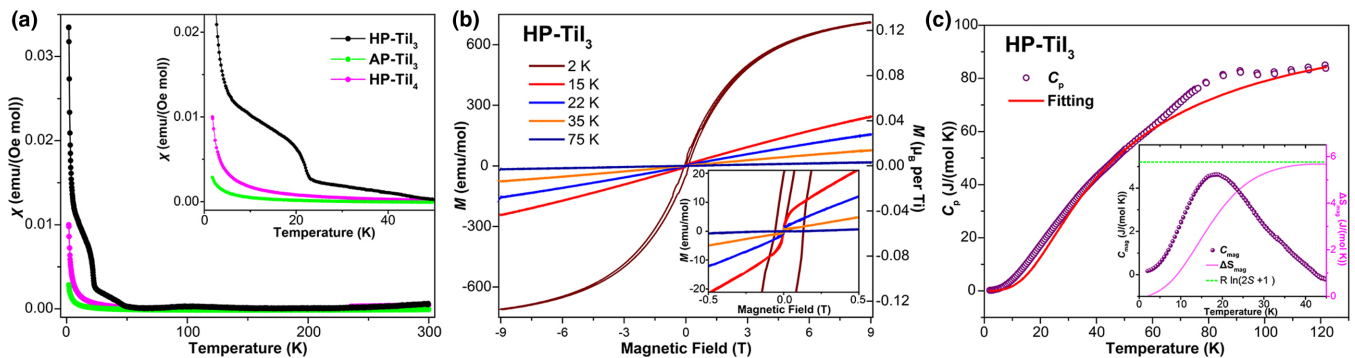

FIG. 4. The magnetic and thermodynamic characterization of TiI$_3$. (a) The temperature-dependent magnetic susceptibility measured with zero-field cooling from 1.8 to 300 K under 1 kOe of HP-TiI$_3$ (black), AP-TiI$_3$ (green), and HP-TiI$_4$ (pink). A 1.8–50 K range is presented in the inset to exhibit the magnetic features. (b) Magnetic moments measured vs magnetic field from −9 to 9 T under different temperatures, on polycrystalline HP-TiI$_3$ powders, with μ_B per Ti unit shown on the right axis. Zoomed-in view of −0.5 to 0.5 T range is shown in the inset. (c) Heat capacity of HP-TiI$_3$ measured under zero field from 2 to 120 K. The red curve represents the Debye model fitting of phonon contribution, with Eq. (1). The subtracted C_{mag} curve is plotted in the inset vs temperature from 2 to 45 K. Corresponding entropy change is exhibited by a pink curve, with a comparison to the value of Heisenberg limit $R \ln(2S + 1) = R \ln(2)$ shown as the green dashed line.

behavior of two-dimensional halides [29], and therefore it may be of future interest to study any potential transitions and low-temperature in-plane rearrangements of the Ti(III) ions in HP-TiI$_3$, as well as their correlation with magnetic properties.

The heat capacity of several HP-TiI$_3$ samples was measured from 1.8 to 120 K, without any magnetic field applied [Fig. 4(c)]. To roughly estimate the magnetic entropy, a fitting of the phonon contribution to the measured heat capacity using the Debye equation [Eq. (1)] was carried out. Considering the large atomic mass difference between titanium and iodine, a modified Debye equation,

$$C_{\text{phonon}} = 9R \sum_{n=1}^{2} C_n \left(\frac{T}{\Theta_{Dn}} \right)^3 \int_0^{\Theta_{Dn}/T} \frac{x^4 e^x}{(e^x - 1)^2} dx, \quad (1)$$

was used, where $C_1 = 1$, with refined values of $\Theta_{D1} = 420.0(6)$ K for titanium, and $C_2 = 3$, with a refined value of $\Theta_{D2} = 148.0(7)$ K for iodine. (A similar modified Debye equation has been applied to fit the phonon heat capacity of other solids with coexisting light and heavy atoms [30,31].) The fitting was applied to the data between 40 and 60 K, which is consistent with the data in the high-temperature range, as shown by the red curve. After subtracting this nonmagnetic contribution from the heat capacity data [Fig. 4(c), inset], a broad peak from 1.8 to 45 K is revealed, which appears to correspond to the magnetic features seen in the magnetic susceptibility data. The broad shape of the estimated C_{mag} transition, as well as the fact that no sharp anomalies are observed in heat capacity data, may be an indication of no long-range magnetic ordering, and that spin-freezing behavior, typical of spin glasses, is observed in this system. The glassiness may be due to either in-plane disorder or magnetic frustration, as the geometrical frustration that results from the triangular lattice as well as the mixture of disordered Ti^{3+} and vacancies may suppress the long-range magnetic order. An estimated entropy change of 5.65 J/(mol K) is calculated based on this transition. This number is very close to the value expected for Heisenberg spins [$R \ln(2S + 1)$] for $S = 1/2$ or Ising spins ($R \ln 2$), and thus it is consistent with the expected electron configuration of Ti(III). An additional peak in the heat capacity is observed at around 85 K, which may correspond to a structural transition. It is known that the honeycomb layered polymorphs of the sister compounds TiCl$_3$ and TiBr$_3$ ($\alpha-$TiCl$_3$/$\alpha-$TiBr$_3$) undergo lattice distortions and dimerization at low temperature [32–34]. Thus, transitions are also possible for the layered triiodide, although with a different in-plane lattice it may display different structural and magnetic properties.

Layered Os$_x$Cl$_3$ ($x = 0.825$ [26] or 0.81 [27]) is a similar system, with disordered transition-metal positions in a triangular in-plane lattice, resulting in a CdI$_2$-type average structure. Structural studies on that material reveal the pos-

sibility of short- and long-range vacancy ordering, and further suggest that different in-plane lattice arrangements may be achieved by different synthesis conditions, with an effect on the magnetism. Both Os$_x$Cl$_3$ studies reported the suppression of long-range antiferromagnetic order and small, broad, field-dependent anomalies in the heat capacity, which is comparable to what is reported here for HP-TiI$_3$, reinforcing our observations

IV. CONCLUSIONS

A layered-structure polymorph of titanium triiodide, which has not been reported previously, has successfully been made from the ambient pressure phase by high-pressure, high-temperature annealing. Different from the 1D chain structure reported for ambient pressure TiI$_3$, its structure is determined by SCXRD to be CdI$_2$-type, with a P-3m1 (no. 164) space group and unit cell ($a = 4.012$ Å and $c = 6.641$ Å at 120 K). The Ti site, with 66.7% occupancy on an ideal triangular lattice, may appear to be randomly occupied either due to random stacking of the layers or to in-plane disorder. The magnetic or structural evidence for either of those things is weak at this point, however, and the anomalous magnetic character of this Ti(III) iodide makes the local arrangement of the Ti an important question to address in future work. Our HP-TiI$_4$ samples present a similar structure after the same high-pressure treatment, with a different fraction of metal on the Ti site. An extensive layered triangular solid solution of M_xI$_2$ is proposed. Magnetic susceptibility and heat capacity measurements conducted on HP-TiI$_3$ reveal some magnetic features below 45 K and a large ZFC-FC deviation below 20 K. The polymorphism, structural properties, and unusual thermal and magnetic behavior of this disordered Ti(III) material, which may act as a quantum material at low temperatures due to the low spin involved, may be of interest for further study, although its air-sensitivity may inhibit its characterization by many techniques.

APPENDIX

CCDC deposition number for HP-TiI$_3$ is 2209900, which contains the supplemental crystallographic data for this paper. The data can be obtained free of charge.

[1] C. Li, X. Lu, W. Ding, L. Feng, Y. Gao, and Z. Guo, Formability of ABX$_3$ (X = F, Cl, Br, I) halide perovskites, Acta Cryst. B **64**, 702 (2008).

[2] A. Ferrari, A. Braibanti, and G. Bigliardi, Refinement of the crystal structure of NiCl$_2$ and of unit-cell parameters of some anhydrous chlorides of divalent metals, Acta Cryst. **16**, 846 (1963).

[3] G. Lal, G. K. Chadha, and G. C. Trigunayat, Crystal structures of six new polytypes of cadmium iodide, Acta Cryst. B **27**, 2293 (1971).

[4] S. N. Magonov, P. Zoennchen, H. Rotter, H. J. Cantow, G. Thiele, J. Ren, and M. H. Whangbo, Scanning tunneling and atomic force microscopy study of layered transition metal halides Nb_3X_8 (X = Cl, Br, I), J. Am. Chem. Soc. **115**, 2495 (1993).

[5] K. W. Plumb, J. P. Clancy, L. J. Sandilands, V. V. Shankar, Y. F. Hu, K. S. Burch, H.-Y. Kee, and Y.-J. Kim, α-$RuCl_3$: A spin-orbit assisted mott insulator on a honeycomb lattice, Phys. Rev. B **90**, 041112(R) (2014).

[6] M. A. McGuire, H. Dixit, V. R. Cooper, and B. C. Sales, Coupling of crystal structure and magnetism in the layered, ferromagnetic insulator CrI_3, Chem. Mater. **27**, 612 (2015).

[7] T. Kong, K. Stolze, E. I. Timmons, J. Tao, D. Ni, S. Guo, Z. Yang, R. Prozorov, and R. J. Cava, VI_3—A new layered ferromagnetic semiconductor, Adv. Mater. **31**, 1808074 (2019).

[8] K. Brodersen, Structure of β-$RuCl_3$, RuI_3, $IrBr_3$, and IrI_3, Angew. Chem. Int. Ed. Engl. **7**, 148 (1968).

[9] H. Hillebrecht, T. Ludwig, and G. Thiele, About trihalides with TiI_3 chain structure: Proof of pair forming of cations in β-$RuCl_3$ and $RuBr_3$ by temperature dependent single crystal x-ray analyses, Z. Anorg. Allg. Chem. **630**, 2199 (2004).

[10] G. Natta, P. Corradini, and G. Allegra, The different crystalline modifications of $TiCl_3$, a catalyst component for the polymerization of α-Olefins. I: A-, β-, γ-$TiCl_3$. II: Δ − $TiCl_3$, J. Polym. Sci. **51**, 399 (1961).

[11] J. M. Fletcher, W. E. Gardner, A. C. Fox, and G. Topping, X-ray, infrared, and magnetic studies of α- and β-ruthenium trichloride, J. Chem. Soc. A **0**, 1038 (1967).

[12] D. Ni, K. P. Devlin, G. Cheng, X. Gui, W. Xie, N. Yao, and R. J. Cava, The honeycomb and hyperhoneycomb polymorphs of IrI_3, J. Solid State Chem. **312**, 123240 (2022).

[13] S. D. Stranks and H. J. Snaith, Metal-halide perovskites for photovoltaic and light-emitting devices, Nat. Nanotech. **10**, 391 (2015).

[14] M. A. McGuire, Crystal and magnetic structures in layered, transition metal dihalides and trihalides, Cryst. **7**, 121 (2017).

[15] C. M. Pasco, I. El Baggari, E. Bianco, L. F. Kourkoutis, and T. M. McQueen, Tunable magnetic transition to a singlet ground state in a 2d van der waals layered trimerized kagomé magnet, ACS Nano **13**, 9457 (2019).

[16] S.-H. Baek, S.-H. Do, K.-Y. Choi, Y. S. Kwon, A. U. B. Wolter, S. Nishimoto, J. van den Brink, and B. Büchner, Evidence for a Field-Induced Quantum Spin Liquid in A-$Rucl_3$, Phys. Rev. Lett. **119**, 037201 (2017).

[17] D. Ni, X. Gui, K. M. Powderly, and R. J. Cava, Honeycomb-structure RuI_3, a new quantum material related to α-$RuCl_3$, Adv. Mater. **34**, 2106831 (2022).

[18] J. Geng, I. Neng Chan, H. Ai, K. Ho Lo, Y. Kawazoe, K. Wei Ng, and H. Pan, Magnetic and electronic properties of 2D TiX_3 (X = F, Cl, Br and I), Phys. Chem. Chem. Phys. **22**, 17632 (2020).

[19] Y. Imai, K. Nawa, Y. Shimizu, W. Yamada, H. Fujihara, T. Aoyama, R. Takahashi, D. Okuyama, T. Ohashi, M. Hagihala *et al.*, Zigzag magnetic order in the kitaev spin-liquid candidate material $RuBr_3$ with a honeycomb lattice, Phys. Rev. B **105**, L041112 (2022).

[20] K. Nawa, Y. Imai, Y. Yamaji, H. Fujihara, W. Yamada, R. Takahashi, T. Hiraoka, M. Hagihala, S. Torri, T. Aoyama *et al.*, Strongly electron-correlated semimetal RuI_3 with a layered honeycomb structure, J. Phys. Soc. Jpn. **90**, 123703 (2021).

[21] G. M. Sheldrick, Crystal structure refinement with SHELXL, Acta Cryst. Sect. C **71**, 3 (2015).

[22] J. Angelkort, A. Schönleber, and S. van Smaalen, Low- and high-temperature crystal structures of TiI_3, J. Solid State Chem. **182**, 525 (2009).

[23] E. G. M. Tornqvist and W. F. Libby, Crystal structure, solubility, and electronic spectrum of titanium tetraiodide, Inorg. Chem. **18**, 1792 (1979).

[24] S. I. Troyanov, Crystal structure of low-temperature modification of TiI_4, Zh. Neorg. Khim. **38**, 226 (1993).

[25] R. Kniep, H. J. Beister, and D. Wald, Polymorphie von tellur(iv)-iodid/polymorphism of tellurium(IV) iodide, Z. Naturforsch. B **43**, 966 (1988).

[26] M. A. McGuire, Q. Zheng, J. Yan, and B. C. Sales, Chemical disorder and spin-liquid-like magnetism in the van der waals layered 5d transition metal halide $Os_{0.55}Cl_2$, Phys. Rev. B **99**, 214402 (2019).

[27] K. Kataoka, D. Hirai, T. Yajima, D. Nishio-Hamane, R. Ishii, K. Choi, D. Wulferding, P. Lemmens, S. Kittaka, T. Sakakibara *et al.*, Kitaev spin liquid candidate Os_xCl_3 comprised of honeycomb nano-domains, J. Phys. Soc. Jpn. **89**, 114709 (2020).

[28] S. I. Troyanov and E. M. Snigireva, Crystal structure of transition metal halides $TiCl_4$, α-$TiCl_3$, WCl_4 and TiI_2, Zh. Neorg. Khim. **45**, 652 (2000).

[29] A. B. Georgescu, A. J. Millis, and J. M. Rondinelli, Trigonal symmetry breaking and its electronic effects in the two-dimensional dihalides MX_2 and trihalides MX_3, Phys. Rev. B **105**, 245153 (2022).

[30] L. Ortega-San Martin, J. P. Chapman, L. Lezama, J. Sánchez Marcos, J. Rodríguez-Fernández, M. I. Arriortua, and T. Rojo, Magnetic properties of the ordered double perovskite Sr_2MnTeO_6, Eur. J. Inorg. Chem. **2006**, 1362 (2006).

[31] L. Li, X. Hu, Z. Liu, J. Yu, B. Cheng, S. Deng, L. He, K. Cao, D.-X. Yao, and M. Wang, Structure and magnetic properties of the S = 3/2 zigzag spin chain antiferromagnet $BaCoTe_2O_7$, Sci. China Phys. Mech. Astron. **64**, 287412 (2021).

[32] C. A. Emeis, F. J. Reinders, and E. Drent, Far-infrared investigation of the phase transition at 217 k in layer-structured $TiCl_3$, Solid State Commun. **16**, 239 (1975).

[33] K. Tsutsumi, H. Okamoto, C. Hama, and Y. Ishihara, Magnetic study of a phase transition at 217 k in α-$TiCl_3$, J. Magn. Magn. Mater. **90-91**, 181 (1990).

[34] S. Pei, J. Tang, C. Liu, J. Mei, Z. Guo, B. Lyu, N. Zhang, Q. Huang, D. Yu, L. Huang *et al.*, Orbital-fluctuation freezing and magnetic-nonmagnetic phase transition in α-$TiBr_3$, Appl. Phys. Lett. **117**, 133103 (2020).

[35] Supplemental Material at http://link.aps.org/supplemental/10.1103/PhysRevMaterials.6.124001 for additional crystallographic and structural information (anisotropic thermal parameters, pXRD Le Bail fittings, HAADF-STEM image) of the titanium iodide system, as well as ZFC/FC temperature dependent magnetic susceptibility of HP-titanium triiodide.